Imaging Matrix-Assisted Laser Desorption/Ionization Fourier Transform Ion Cyclotron Resonance Mass Spectrometry of oxaliplatin derivatives in human tissue sections

Justine Ferey, Marion Larroque, Isabelle Schmitz-Afonso, Johann Le Maître, Olivia Sgarbura, Sébastien Carrere, François Quenet, Brice Bouyssière, Christine Enjalbal, Sandra Mounicou, et al.

Imaging Matrix-Assisted Laser Desorption/Ionization Fourier Transform Ion Cyclotron Resonance Mass Spectrometry of oxaliplatin derivatives in human tissue sections

Justine Ferey[1,2,3], Marion Larroque[4], Isabelle Schmitz-Afonso[1*], Johann Le Maître[1], Olivia Sgarbura[5], Sébastien Carrere[5], François Quenet[5], Brice Bouyssiere[6], Christine Enjalbal[7], Sandra Mounicou[6], Carlos Afonso[1]

[1]Normandie Univ, COBRA, UMR 6014 and FR 3038, Université de Rouen, INSA de Rouen, CNRS, IRCOF, 1 rue Tesnières, 76821 Mont-Saint-Aignan, Cedex, France.
[2]UMR1331 Toxalim (Research Centre in Food Toxicology), Toulouse University, INRAE, ENVT, INP-Purpan, UPS, 31027 Toulouse, France
[3] Metatoul-AXIOM platform, National Infrastructure for Metabolomics and Fluxomics: MetaboHUB, Toxalim, INRAE, 31027 Toulouse, France
[4]Unité de Recherche Translationnelle, Institut du Cancer de Montpellier (ICM), 208 rue des apothicaires, 34298 Montpellier, France.
[5]Service Chirurgie, Institut du Cancer de Montpellier (ICM), 208 rue des apothicaires, 34298 Montpellier, France.
[6]Universite de Pau et des Pays de l'Adour, E2S UPPA, CNRS, IPREM, Institut des Sciences Analytiques et de Physico-chimie pour l'Environnement et les Materiaux, UMR5254, Hélioparc, 64053 Pau, France
[7]Univ Montpellier, IBMM, CNRS, ENSCM, 34095 Montpellier, France

*Corresponding author at: Normandie Univ, COBRA, UMR 6014 and FR 3038, Université de Rouen, INSA de Rouen, CNRS, IRCOF, 1 rue Tesnières, 76821 Mont-Saint-Aignan, Cedex, France. E-mail address : isabelle.schmitz-afonso@univ-rouen.fr

Abstract

Mass Spectrometry Imaging is an effective technology that allows to determine the *in-situ* distribution of endogen and/or exogen small molecules. It is a rapidly emerging approach for visualizing drugs and their metabolites within biological tissues. Matrix-Assisted Laser Desorption Ionization (MALDI) Mass Spectrometry Imaging (MSI) coupled to high resolving power analyzer (e.g. TOF) was already investigated for metallodrug localization and metabolization studies, but was proved to suffer from a lack of sensitivity and resolution, leading to poor coverage and assignment. To counter these technological limitations, the use of ultra-high resolving power analyzer such as Fourier Transform Ion Cyclotron Resonance (FTICR) could be revealed as a technique of choice. The high field FTICR MS provides ultra-high resolving power and mass accuracy that allows exhaustive molecule coverage and non-ambiguous molecular formula assignments. Platinum derivatives, such as oxaliplatin, are widely used as therapeutic agents for cancer treatment. The assessment of their intake, distribution and metabolism within the organs is important to know the risks associated with their use. In this study, MALDI FTICR MSI analyses were performed to better understand the penetration and metabolization of platinum derivatives in ovaries of women treated by Hyperthermic Intraperitoneal Chemotherapy (HIPEC) for peritoneal metastasis of colorectal or appendicular origin. Twelve ovary sections, from six ovary samples in six women donors, before and after treatment, were analyzed with 120 µm spatial resolution. For the first time, the high resolving power (220,000 at *m/z* 457) and sub-ppm accuracy (< 1 ppm) of the FTICR combined with an Isotopic Fine Structure study enabled to distinguish two Pt-isobaric species derived from oxaliplatin in biological tissues. One of these, which is unknown, was specifically localized at the contour of the ovary.

Keywords : Mass Spectrometry Imaging; MALDI-FTICR ; ovary ; platinum metabolites ; HIPEC ; Isotopic Fine Structure

1. Introduction

Mass Spectrometry Imaging (MSI) has entered the field of tissue-based research. It is an effective technology that allows to determine the *in-situ* distribution of endogen and/or exogen small molecules. Introduced by Caprioli et al [1], MSI using Matrix-Assisted Laser Desorption/Ionization Time-Of-Flight (MALDI-TOF) technology has become an appropriate alternative to radioactive labeling, to visualize simultaneously initial drug distribution and their metabolism in specific tissues or whole animal body [2]. This became possible by spatially imaging the mass to charge (*m/z*) ratios of molecules to generate molecular pictures of the tissue [1]. Currently, application of MALDI MSI in drug research and development has attracted intense attention from the pharmaceutical industry [3, 4]. MALDI imaging is complementary to more conventional optical imaging techniques (such as histology, fluorescence, RAMAN microscopy, Xray spectroscopy [5]) and lies in its label-free, unparalleled chemical information and spatially resolved detection. In this way, the MSI technique is raising interest, especially in clinical research, for various kinds of applications like drug biodistribution and metabolization studies. However, it must be noted that the use of Formalin-Fixed Paraffin-Embedded (FFPE) tissues is not recommended for metabolite studies (loss and delocalization of the metabolites during the washing steps), which may reflect a limitation of this technique regarding the large FFPE samples library. This limitation is of less importance for MSI of proteins, more robust to FFPE sample preparation steps. [6, 7]

In particular, platinum-based drugs play an important role in cancer treatment [8, 9]. Given the clinical use of these drugs, evaluation of their intake, distribution and metabolism within organs and/or tumors is important to study the efficacy, metabolization and the fate of the drug in the organism. Various methodological developments for the imaging of this metal-based anti-

cancer compound as Pt-metallodrugs in biological samples were improved in the last years [10]. The main analytical tools for MS-based metallodrug imaging related in the literature are SIMS-MSI, LA-ICP-MSI and MALDI-MSI. These three techniques can be compared in term of sensitivity, spatial resolution and type of analytes detected. While SIMS-MSI and MALDI-MSI are useful in providing molecular information on the drug metabolites, they suffer from a lower sensitivity than LA-ICP-MS [10-12]. Indeed, LA-ICP-MS technique is very sensitive (platinum detection around ng/mg of tissue [13]), offers a spatial resolution of 1 µm, does not require chemical derivatization of the sample, allows for FFPE sections analysis but does not allow molecular characterization of the metallodrug. Besides, SIMS-MSI offers the best spatial resolution (100 nm) with a sensitivity up to 0.1 pg/mg of tissue [5] for elemental and molecular fragments while MALDI-MSI provides the visualization of biomolecules leading to molecular information on intact drug species formed, at the µm scale. However, MALDI-TOF MSI [14] shows low sensitivity (picogram level detection) for platinum compound detection due to poor ionization of metallodrugs in comparison to LA-ICP-MSI. As detailed below, MALDI-MSI limitations can be overcome thanks to FTICR instruments instead of TOF analyzers.

Nowadays, oxaliplatin is the most administrated anti-cancer drug of all platinum based-treatments and the study of its metabolization, as oxaliplatin-methionine complex metabolite, is of great interest **(formulas shown in Figure 1).**

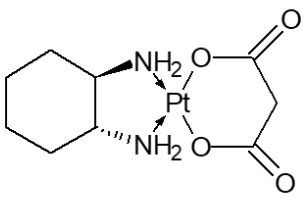

Chemical Formula $C_8H_{14}N_2O_4Pt$
Exact Mass: 397.0601
Oxaliplatin

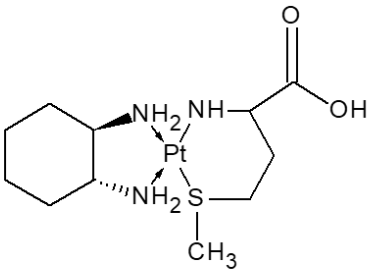

Chemical Formula $C_{11}H_{23}N_3O_2PtS$
Exact Mass: 456.1159
Oxaliplatin-methionine

Figure 1: Structural formulas of oxaliplatin and oxaliplatin-methionine.

Indeed, a MALDI TOF-MSI approach has been previously developed to study the distribution of oxaliplatin in rat kidney, in which platinum-containing compounds were detected as complexes that might be attributed to oxaliplatin-methionine and oxaliplatin-cysteine [15]. These findings were complemented by a combined MALDI-TOF and LA ICP-MS imaging in which the presence of platinum drugs was confirmed in human tumors [16] and in ovaries [13] from HIPEC treated patients. However, in many cases, *in vivo* administrated drugs can be more difficult to analyze than endogenous small molecules due to their low abundance (ng/mg of platinum in the ovaries [13]) and due to the ionization competition phenomenon with more abundant and more easily ionizable molecules. In addition, the mass resolution of the TOF MS instruments (typically between 20,000 to 50,000) may not be sufficient to separate all isobaric species in the absence of prior chromatographic separation [17]. Consequently, in some cases, it is not possible to evidence the presence of some species when high abundance isobars are present. Therefore, it is difficult to precisely identify individual signal in MSI spectra and resulting MS/MS experiments are the combination of fragments from several isobaric precursor ions [18].

The MALDI-TOF-MSI tool limitations [13] can be overcome with the use of ultra-high resolution mass analyzer such as Fourier Transform Ion Cyclotron Resonance (FTICR) MS [19-21]. High resolution instruments are defined by a resolving power, Full Width at Half Maximum (FWHM), above 10,000 [22] whereas ultra-high resolution analyzers provide a resolving power above 200,000 [17]. Thus, the FTICR MSI at high magnetic field provides high mass accuracy (< 1 ppm) and ultra-high resolving power (> 200,000) enabling the separation of most isobaric species. In addition, the resolution obtained during FTICR MS tissue imaging is very suitable for unambiguous molecular formula attribution taking advantage

of the Isotopic Fine Structure (IFS) [17-19, 23-26]. Therefore, this technique is of great interest for exhaustive analysis, rapid and precise annotation of compounds in biological samples [27] and already have proved its merit for MALDI imaging analysis of biological tissues in terms of resolving power, mass accuracy and dynamic range [27].

In this way, the objective of this study was to investigate the insight of MALDI-MSI coupled to FTICR analyzer for the visualization and the identification of oxaliplatin and its potential metabolites in human ovary surgically resected from woman treated with HIPEC for a peritoneal carcinomatosis. Briefly, peritoneal carcinomatosis is a common extension of colon cancer whose recurrence is characterized by the multiplication of tumor nodules on the peritoneum. HIPEC is one of the most recent treatments enabling a significantly improved survival of the patients. It consists in a local application of a high concentration of warmed anti-cancer Pt-metallodrugs, such as oxaliplatin, through the peritoneal cavity [28-31]. In treated women, the intra peritoneal location of ovaries raises the possibility for their contamination with the Pt-drug [13]. Thus, the objective of the related clinical work is to optimize oxaliplatin distribution to tumoral nodules issued from peritoneal metastasis during the HIPEC while limiting its diffusion to adjacent organs like ovaries in order to preserve fertility. The eventual contamination of the ovaries has been studied in this work. As a result, the analyses of 12 ovary sections before and after treatment enabled to highlight the presence of a Pt-metabolite on the outskirts of the organ. The ultra-high mass accuracy and resolution of the FTICR analysis combined with the study of IFS allowed to determine with a high level of confidence the molecular formula of this Pt-containing metabolite, derived from oxaliplatin.

2. Materials and Methods

2.1. Reagents and chemicals

Acetonitrile (ACN) and water quality grade LC-MS were purchased from Fisher Scientific (Loughborough, UK). α-Cyano-4-hydroxycinnamic acid (CHCA) matrix, and trifluoroacetic acid (TFA), were purchased from Sigma-Aldrich (S^t Louis, US). Sodium trifluoroacetate (NaTFA, Sigma-Aldrich, S^t Louis, US), at a concentration of 0.1 mg mL^{-1} (ACN/H_2O 50/50 (v/v)) was used as external calibrant before each analysis. Oxaliplatin-methionine was prepared by reacting Eloxatin solution (1.3mM) with the amino acid methionine (1.3mM) in physiological buffer (23mM $NaHCO_3$, 5mM NaH_2PO_4, pH7.4) at 37°C under 5% CO_2 for 24h. All chemicals and solvents for this reaction were purchased from Sigma Aldrich (St. Louis, MO. USA) [15].

2.2. Tissue collection

For this prospective study, all patients gave written informed consent before the procedure, and the institutional review board approved the study, which was performed in accordance with the ethical standards of the Helsinki Declaration of 1975. Six ovary samples were surgically removed from women donors diagnosed with colorectal peritoneal carcinomatosis before and after HIPEC treatment of the peritoneal tumoral nodule with oxaliplatin drug. Clinical patient's data and HIPEC treatments were previously published [13]. Briefly, the patients in this group presented peritoneal metastasis of colorectal (4 patients) and appendicular (2 patients) origin. The appendicular origin was low grade appendiceal mucinous neoplasm (LAMN) [32]. The two entities were included as the HIPEC protocol is similar, based on the administration of oxaliplatin. The prognostic of the two entities, however, is quite different with a median overall survival (OS) of 41.7 months for the patients with peritoneal metastasis of colorectal origin, while it is of 196 months for patients with LAMN [32, 33]. The difference of prognosis of these patients has no impact on the results of the current study that aims to detect penetration of the ovaries. This latter aspect can be highly important for the female patients that have fertility

projects that are compatible with the long survival of some of these patients [34]. For each donor, one ovary was removed before HIPEC treatment and used as a reference sample for MALDI-FTICR MSI. The ones removed after treatment were used to image the drug localization and to identify the drug metabolite. In addition, one peritoneal tumoral nodule section was also sampled for analysis. The samples were frozen in liquid nitrogen and stored at -80°C until analysis.

2.3. Tissue preparation for MALDI FTICR imaging

Fresh frozen 10 µm ovary sections were obtained with a Microm HM 550 cryotome (Thermo Scientific, Germany) using -18°C and -20°C temperatures for the specimen and the chamber respectively. Sections were mounted on conductive Indium tin oxide (ITO)-coated slides (Bruker, Bremen, Germany, 75x50 mm) and stored at -80°C. Before analysis, the slides were first taken back at room temperature for 1h in a desiccator. CHCA matrix solution (5 mg mL^{-1} in ACN/H_2O 70/30 (v/v), 0.1% TFA) was applied to the tissue sections with an automatic microsprayer HTX TM-Sprayer (HTX Imaging, Chapel Hill, NC, US) with the following parameters: flow rate 100 µL min^{-1}, number of passes 12, track spacing 2 mm, nozzle temperature 85°C, nozzle velocity 1200 mm min^{-1}, N_2 pressure 10 psi and N_2 flow rate 2 L min^{-1}. Slides were dried under vacuum before analysis.

2.4. Mass spectrometry instrumentation

MALDI imaging analyses were performed on a FTICR instrument (solariX XR, Bruker, Bremen, Germany) equipped with a 12 Tesla superconducting magnet and a dynamically harmonized ICR cell. This instrument is equipped with both laser desorption ionization source (smartbeam II, 1 kHz Nd:YAG×3 laser at 355 nm, Bruker) and an electrospray ionization (ESI) source. Mass spectrometric analyses were performed in positive ion mode in the mass range *m/z* 150-1000. Each MALDI mass spectrum for each position is the result of 250 consecutive

laser shots. Spectra were acquired with a 120 µm spatial resolution. The analytical resolution is 220,000 at *m/z* 457.

Before each image acquisition, external calibration was performed in positive ion mode by NaTFA infusion *via* ESI source. Internal calibration of the MALDI mass spectra was then performed by assigning known metabolites in the mass range *m/z* 150-1000. During the image acquisition, an auto-calibration was performed assigning $C_5H_{14}NO_4P$ (*m/z* 184.07332, $[M+H]^+$, phosphocholine), $C_{10}H_7NO_3$ (*m/z* 399.03778, $[2M+K]^+$, matrix peak), $C_{24}H_{50}NO_7P$ (*m/z* 496.33977, $[M+H]^+$, lipid), $C_{37}H_{75}N_2O_6P$ (*m/z* 675.54355, $[M+H]^+$, lipid), $C_{42}H_{82}NO_8P$ (*m/z* 782.56703, $[M+Na]^+$, lipid), $C_{44}H_{80}NO_8P$ (*m/z* 820.52531, $[M+K]^+$, lipid).

Data size was set at 2 million points for a transient length of 0.87 s and mass spectra were acquired with a 97% data file reduction. All images were acquired with the FTMS control and FlexImaging (v 5.0, Bruker, Bremen) softwares. Images were processed with SCiLs Lab Pro software (Bruker Daltonics, Bremen, Germany).

To unambiguously determine the molecular formula of the compound of interest, the IFS was evaluated by accumulation of 20 scans on the region of interest by zone profiling. Molecular formulas were generated using Bruker Data Analysis, considering the following elements and limits ($C_{0-20}H_{0-40}O_{0-10}N_{0-10}S_{0-4}Pt_{0-1}$) with *m/z* errors < 1 ppm.

3. Results and discussions

3.1. Pt localization inside ovary tissues

The aim of the study is to localize and identify by MALDI-FTICR MSI analysis the administrated Pt-drug and/or its metabolites after HIPEC treatment of the peritoneal metastasis in adjacent ovarian tissue section. Mass spectrum of a Pt-containing compound has a characteristic isotopic profile, characterized by the *m/z* values of each isotope. This profile is due to the presence of the three most abundant platinum isotopes namely ^{194}Pt, ^{195}Pt and ^{196}Pt

with respective relative abundance of 32.9%, 33.9% and 25.9%. For the 6 patients, one ovary was removed before HIPEC treatment (reference tissue) and the other one after treatment. Overall, 12 ovary sections were analyzed. Due to the high number of detected metabolites (more than 1,200 peaks for an ovary tissue analysis), the isotope profile of Pt-compounds is difficult to detect. To evidence Pt-containing compounds, a non-targeted search of discriminating *m/z* values was carried out between the sections before and after treatment, with SCiLS software.

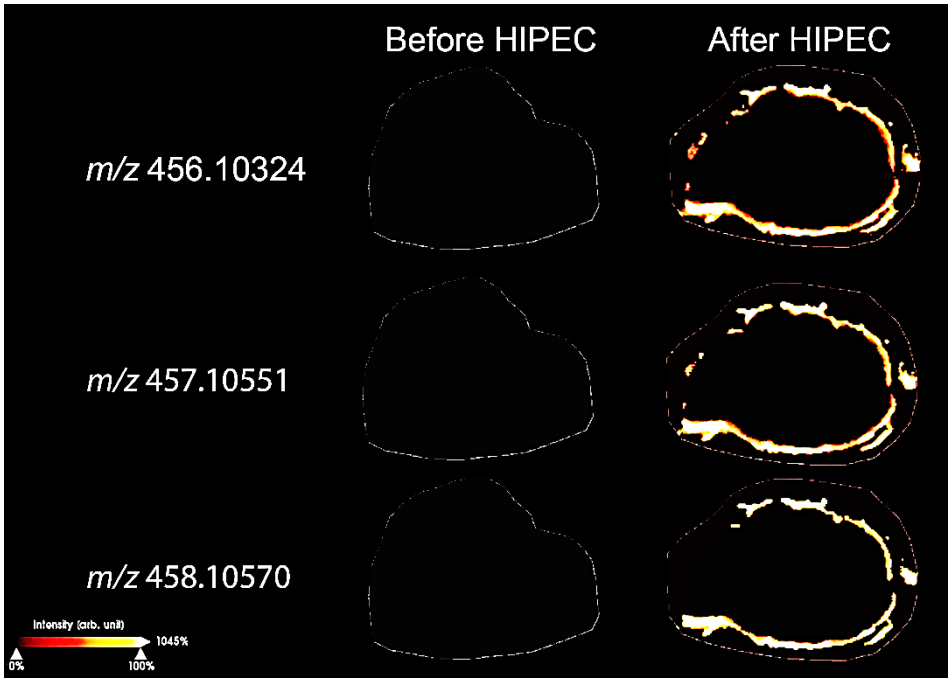

Figure 2: MALDI FTICR MSI of ovary tissues before and after HIPEC treatment. Visualization of discriminative values at *m/z* 456.10324, *m/z* 457.10551 and *m/z* 458.10570. Spatial resolution of 120 µm.

In Figure 2, MALDI FTICR MS images show a peripheral location of a discriminative compound at three *m/z* values, *m/z* 456.10324, *m/z* 457.10551 and *m/z* 458.10570, which do not correspond to the original oxaliplatin compound (*m/z* 397.0653, *m/z* 398.0675, *m/z* 399.0679). The same peripheral distribution could indicate that they are from the same molecule. Moreover, the nominal masses of these three *m/z* values are separated by one mass unit, which could reflect the presence of the platinum isotopic profile.

3.2. Determination of molecular formula of peripheral Pt-based compound by FTICR

With ultra-high resolution instruments, the molecular formula of a compound can be determined thanks to a high mass accuracy and to an isotopic pattern study [24]. To get a higher signal to noise ratio and therefore better define the isotopic structure, 20 spectra were accumulated in the peripheral regions of the tissue.

The three detected masses at *m/z* 456.10324, *m/z* 457.10551 and *m/z* 458.10570 did not correspond to the oxaliplatin ion. With a mass difference of 40 ppm, this species is an isobar of the oxaliplatin-methionine complex $C_{11}H_{23}N_3O_2SPt$ (**Figure 1, Table 1)** described in the study of Bouslimani *et al.* [15]. The resolution, around 20,000, and mass measure precision, difference of 0.06 Da, would not have been sufficient in this study to differentiate the two isobars. Thus, to validate the presence of another compound than oxaliplatin-methionine in these tissue sections, drops of 1 µL of this complex were deposited at the tissue peripheries. As shown in **Figure S1**, the FTICR high resolution (220,000 at *m/z* 457.12309) enabled to distinguish these two isobaric species. The overall internally calibrated mass spectrum showed an average error of 0.133 ppm in the mass range *m/z* 150-1000. From this accurate mass measurement, the molecular formula of oxaliplatin-methionine complex was confirmed ($^{12}C_{11}{}^{1}H_{23}{}^{14}N_3{}^{16}O_2{}^{32}S{}^{195}Pt$) with a mass accuracy of 0.453 ppm. This statement was reinforced by the analysis of a section from a peritoneal tumoral nodule itself, resected after HIPEC. Results, shown in **Figure S2**, highlight the presence of three oxaliplatin-methionine complex isotopes (**Table 1**) as previously described [15], with respective errors of 0.145 ppm, 0.060 ppm and 0.388 ppm. As shown in **Figure S3**, the other platinum complex at *m/z* 457.10551 was also visualized in these tissues after HIPEC treatment with the presence of the three co-localized isotopes ^{194}Pt, ^{195}Pt, and ^{196}Pt.

	^{194}Pt (M) [M+H]+	**^{195}Pt (M+1) [M+H]+**	**^{196}Pt (M+2) [M+H]+**
Oxaliplatin $^{12}C_8{}^{1}H_{14}{}^{14}N_2{}^{16}O_4Pt$	397.065314	398.067522	399.067585
Oxaliplatin-methionine	456.121055	457.123297	458.123319

$^{12}C_{11}{}^{1}H_{23}{}^{14}N_3{}^{16}O_2{}^{32}SPt$

Table 1: Theoretical *m/z* values of the isotopes M (^{194}Pt), M+1 (^{195}Pt) and M+2 (^{196}Pt) for oxaliplatin and oxaliplatin-methionine complex.

The use of high field FTICR analyzer, providing high mass accuracy and resolution, was demonstrated to be essential for the unambiguous differentiation of these isobaric compounds, which reveals the presence of a platinum-derivative at the contours of the ovary.

In the ovary tissue sections mass spectra, the molecular formula of the ion of interest was determined from the monoisotopic peak, calculated by using the most abundant isotope of each element (*m/z* 457.10551 for ^{195}Pt). Then, the molecular formula of this compound was precisely determined by study of the IFS. In major cases, mass spectrometry studies have to consider atomic isotopes that play an important role in the atomic elucidation of a compound. Generally, each element has one most abundant isotope (such as ^{12}C) and others with minor abundance (such as ^{13}C). These low abundance isotopic peaks can be separated from other isobaric isotopologues when working at sufficiently high resolution, thus facilitating the atomic composition determination [27]. Primary, the high mass accuracy of the spectrum considerably reduced the number of possible molecular formulas especially for Pt-containing compound. The monoisotopic peak detected at *m/z* 457.10551 had 3 candidate formulas, namely $C_{10}H_{19}N_3O_5Pt$, $C_{11}H_{15}N_7OPt$ and $C_{11}H_{23}N_3S_2Pt$, at respective mass errors of −1.86, 1.09 and 0.06 ppm **(Table 2).** The mass accuracy of each isotopologue (containing ^{194}Pt, ^{195}Pt and ^{196}Pt) and their relative intensity were compared to the theoretical mass spectra, generated at the same resolving power as the experimental mass spectrum (220,000). All *m/z* values and relative intensities of the clearly resolved isotope peaks are listed in **Table 2**.

		^{194}Pt (M)	**^{195}Pt (M+1)**	**^{196}Pt (M+2)**
Theoretical *m/z* (relative abundance)	$^{12}C_{10}{}^{1}H_{19}{}^{14}N_3{}^{16}O_5Pt$	456.10243 (87%)	457.10466 (100%)	458.10472 (68%)
	$^{12}C_{11}{}^{1}H_{15}{}^{14}N_7{}^{16}OPt$	456.10376 (87%)	457.10601 (100%)	458.10604 (68%)
	$^{12}C_{11}{}^{1}H_{23}{}^{14}N_3{}^{32}S_2Pt$	456.10330 (87%)	457.10554 (100%)	458.10555 (68%)

Experimental *m/z* (relative abundance)		456.10324 (93%)	457.10551 (100%)	458.10570 (70%)
Errors between theoretical and experimental values (ppm)	$^{12}C_{10}{}^{1}H_{19}{}^{14}N_{3}{}^{16}O_{5}Pt$	-1.78	-1.86	-2.19
	$^{12}C_{11}{}^{1}H_{15}{}^{14}N_{7}{}^{16}OPt$	1.15	1.09	0.736
	$^{12}C_{11}{}^{1}H_{23}{}^{14}N_{3}{}^{32}S_{2}Pt$	0.125	0.06	-0.319

Table 2: Theoretical and experimental *m/z* values and relative abundance (%) of the isotopes M (^{194}Pt), M+1 (^{195}Pt) and M+2 (^{196}Pt) for the determined raw formulas $C_{10}H_{19}N_3O_5Pt$, $C_{11}H_{15}N_7OPt$ and $C_{11}H_{23}N_3S_2Pt$ of the unknown compound with associated *m/z* errors.

Figure 3 shows the complete pattern spectra containing the M (^{194}Pt), M+1 (^{195}Pt) and M+2 (^{196}Pt) isotopes for the experimental analysis and the simulated patterns with an expanded window of the monoisotopic peak M+1. For the three molecular formulas, the three isotopes are present in the spectra with excellent mass accuracies **(Table 2).** The experimental relative abundances are adequate with the theoretical ones with 93%, 100% and 70% for M, M+1 and M+2 isotope, respectively. The precise identification was therefore performed by studying the IFS of the M+2 isotope showing three resolved isotopologues. As shown in **Figure 4,** for each molecular formula, we observed a peak generated by ^{13}C substitution (*m/z* 458.10796 for $^{12}C_9{}^{13}C_1{}^{1}H_{19}{}^{14}N_3{}^{16}O_5{}^{195}Pt$, *m/z* 458.10930 for $^{12}C_{10}{}^{13}C_1{}^{1}H_{15}{}^{14}N_7{}^{16}O{}^{195}Pt$ and *m/z* 458.10882 for $^{12}C_{10}{}^{13}C_1{}^{1}H_{23}{}^{14}N_3{}^{32}S_2{}^{195}Pt$). The experimental one is observed at *m/z* 458.10853. For $C_{11}H_{23}N_3S_2Pt$, the peak observed at *m/z* 458.09909 is produced by a ^{34}S substitution. This peak is also encountered in the experimental profile at *m/z* 458.09967 which proves the presence of sulfur in the compound. The peak caused by a ^{34}S substitution (*m/z* 458.09909) is resolved from the peaks caused by a ^{196}Pt substitution (*m/z* 458.10555) and a $^{195}Pt^{13}C$ substitution (*m/z* 458.10882). This isotope study also confirmed the presence of platinum. This IFS confirmed the molecular formula $C_{11}H_{23}N_3S_2Pt$ that does not fit with the oxaliplatin-methionine compound previously reported to be identified in rat tumoral kidney tissue and in tumoral peritoneum tissue [15]. Consequently, we could confirm the presence of oxaliplatin-methionine in tumoral peritoneum tissue but not in the ovary tissue sections from the treated women, implying that the Pt-drug diffuses to the ovary with the metabolization of another compound. These results

were confirmed by measurements on tissue from six patients. Platinum metabolite distribution in the 6 ovary sections before treatment and 6 ovary sections after treatment is shown in **Figure S4**. MSI based on FTICR mass analyzer showed here its great potential for unambiguous metabolite identification.

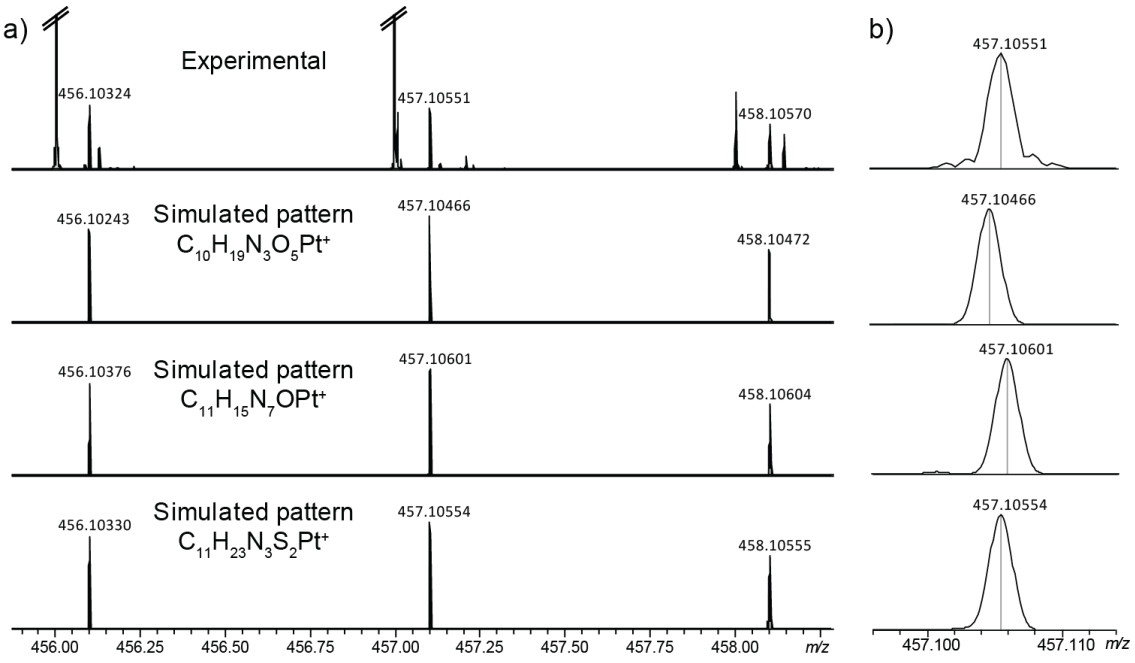

Figure 3: MALDI FTICR MS spectra of (a) Experimental and theoretical isotopic distribution patterns of $C_{10}H_{19}N_3O_5Pt$, $C_{11}H_{15}N_7OPt$ and $C_{11}H_{23}N_3S_2Pt$ for M (^{194}Pt), M+1 (^{195}Pt) and M+2 (^{196}Pt) isotopes (b) expanded *m/z* window of the experimental monoisotopic peak at *m/z* 457,10551 and the three theoretical monoisotopic peaks of $C_{10}H_{19}N_3O_5Pt$, $C_{11}H_{15}N_7OPt$ and $C_{11}H_{23}N_3S_2Pt$.

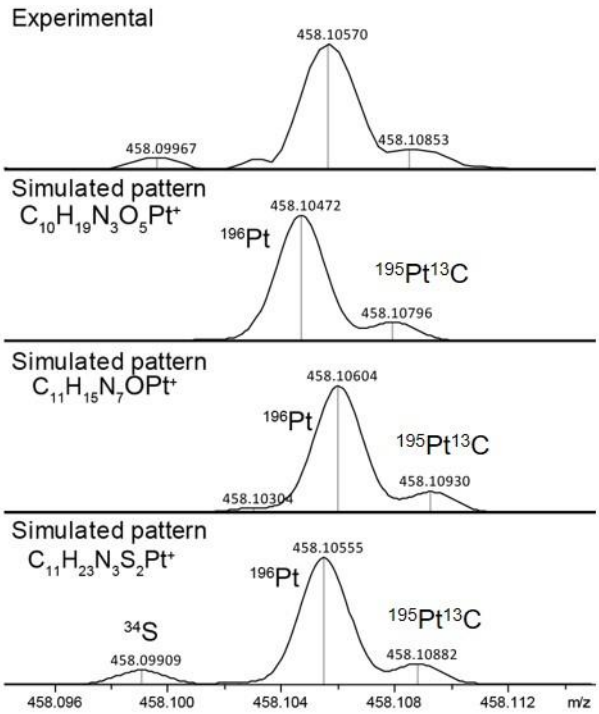

Figure 4: MALDI FTICR MS spectra of observed and theoretical isotopic fine structure of $C_{10}H_{19}N_3O_5Pt$, $C_{11}H_{15}N_7OPt$ and $C_{11}H_{23}N_3S_2Pt$ for M+2 (^{196}Pt).

Although the confirmation of a developed structural formula could not be performed by tandem MS/MS mass spectrometry due to the very low signal intensity of the Pt compound, hypothesis could be made from the literature.

Previously reported platinum and sulfur containing complexes were described, involving the formation of a complex with a diethyldithiocarbamate (DDTC) molecule [14]. According to the determined molecular formula, we can hypothesize that the DACH (diaminocyclohexane)-Pt group has complexed with a DDTC molecule to form the complex (DACH) (DDTC) Pt(II) **(Figure S5).** Even if DDTC acts as rescue agent, recommended by the World Health Organization, to detoxify platinum after chemotherapy treatment, to our knowledge, this molecule was not administrated during HIPEC [35-37]. In other way, the presence of DDTC could come from its use as a pesticide. Some studies revealed the accumulation and the effect

of this kind of carbamates on the male and female reproductive organs [38, 39]. Nevertheless, its presence as a complex into the ovaries after (during) an HIPEC procedure would need to be confirmed by complementary studies to assign the detected Pt-containing compound. Further investigations have to be carried out to formally identify the structure of this Pt metabolite ($C_{11}H_{23}N_3S_2Pt$ molecular formula) and explain its origin.

Therefore, this study showed that oxaliplatin still diffuses to the non-diseased ovarian tissues despite HIPEC optimization. It highlighted the great interest of FTICR-MSI to help in optimizing treatment protocols by understanding drug metabolism and fate in living cells.

4. Conclusion

This study showed that detailed characterization of biological samples by MALDI imaging can require instrumentation with high mass resolving power and mass accuracy. This work shows the potential of MALDI imaging coupled to FTICR analyzer for the non-targeted study of Pt-drug in ovary tissue after HIPEC treatment of the peritoneal metastasis. The high mass accuracy and resolving power allowed to distinguish the presence of two Pt-isobars. Both the oxaliplatin-methionine complex and the new isobaric complex were detected in the tumoral peritoneal tissue whereas the new complex only was localized at the periphery of the ovary. The use of lower resolution mass analyzer such as TOF, would not allow the separation of these isobaric species, leading to wrong assignments. The molecular formula of this unknown compound was then determined thanks to high mass accuracy and high resolution enabling an isotopic fine structure study. To our knowledge, this study showed for the first time the powerful of MALDI FTICR MS for imaging and molecular elucidation of metallodrug species in treated biological tissues. Besides, it showed, for the first time, the presence of an unknown Pt-species in ovary tissues after HIPEC treatment, which open new perspective in the study of Pt-metallodrug metabolization understanding.

Acknowledgments

This work has been partially supported by University of Rouen Normandy, INSA Rouen Normandy, the Centre National de la Recherche Scientifique (CNRS), European Regional Development Fund (ERDF), Labex SynOrg (ANR-11-LABX-0029), Carnot Institute I2C, the graduate school for research XL-Chem (ANR-18-EURE-0020 XL CHEM), and by Région Normandie. This work was supported the European Union's Horizon 2020 Research Infrastructures program (Grant Agreement 731077). Access to a CNRS FTICR research infrastructure (FR3624) is gratefully acknowledged.

Competing interest

The authors declare no competing financial interest.

Appendix A. Supplemental information.

Supplementary data associated with this article can be found in the online version at ….

References

[1] R.M. Caprioli, T.B. Farmer, J. Gite, Molecular imaging of biological samples: localization of peptides and proteins using MALDI-TOF MS, Anal. Chem. 69 (1997) 4751-4760. https://doi.org/10.1021/ac970888i

[2] S. Khatib-Shahidi, M. Andersson, J.L. Herman, T.A. Gillespie, R.M. Caprioli, Direct Molecular Analysis of Whole-Body AnimalTissue Sections by Imaging MALDI MassSpectrometry, Anal. Chem 78 (2006) 6448-6456. https://doi.org/10.1021/ac060788p

[3] S. Schulz, M. Becker, M.R. Groseclose, S. Schadt, C. Hopf, Advanced MALDI mass spectrometry imaging in pharmaceutical research and drug development, Curr. Opin. Biotechnol. 55 (2019) 51-59. https://doi.org/10.1016/j.copbio.2018.08.003

[4] Y. Hsieh, J. Chen, W.A. Korfmacher, Mapping pharmaceuticals in tissues using MALDI imaging mass spectrometry, J. Pharmacol. Toxicol. Methods 55(2) (2007) 193-200. https://doi.org/10.1016/j.vascn.2006.06.004

[5] D.J. Hare, E.J. New, M.D. de Jonge, G. McColl, Imaging metals in biology: balancing sensitivity, selectivity and spatial resolution, Chem. Soc. Rev. 44(17) (2015) 5941-58. https://doi.org/10.1039/C5CS00055F

[6] A. Ly, A. Buck, B. Balluff, N. Sun, K. Gorzolka, A. Feuchtinger, K. P. Janssen, P. J. K. Kuppen, P. J. K. Kuppen, C. J. H. Van de Velde, G. Weirich, F. Erlmeier, R. Langer, M. Aubele, H. Zitzelsberger, L. McDonnell, M. Aichler, A. Walch, High-mass-resolution MALDI mass spectrometry imaging of metabolites from formalin-fixed paraffin-embedded tissue, Nat. Protoc 11 (2016) 1428-1443. https://doi.org/10.1038/nprot.2016.081

[7] J. Stauber, R. Lemaire, J. Franck, D. Bonnel, D. Croix, R. Day, M. Wisztorski, I. Fournier, M. Salzet, MALDI Imaging of Formalin-Fixed Paraffin-Embedded Tissues: Application to Model Animals of Parkinson Disease for Biomarker Hunting, J. Proteome Res. 7(3) (2008) 969-978. https://doi.org/10.1021/pr070464x
[8] T. Makovec, Cisplatin and beyond: molecular mechanisms of action and drug resistance development in cancer chemotherapy, Radiol. Oncol. 53(2) (2019) 148-158. https://doi.org/10.2478/raon-2019-0018
[9] S.J. Park, W. Ye, R. Xiao, C. Silvin, M. Padget, J.W. Hodge, C. Van Waes, N.C. Schmitt, Cisplatin and oxaliplatin induce similar immunogenic changes in preclinical models of head and neck cancer, Oral oncol. 95 (2019) 127-135. https://doi.org/10.1016/j.oraloncology.2019.06.016
[10] S. Theiner, A. Schoeberl, A. Schweikert, B.K. Keppler, G. Koellensperger, Mass spectrometry techniques for imaging and detection of metallodrugs, Curr Opin Chem Biol 61 (2021) 123-134. https://doi.org/10.1016/j.cbpa.2020.12.005
[11] R.F.S. Lee, S. Theiner, A. Meibom, G. Koellensperger, B.K. Keppler, P.J. Dyson, Application of imaging mass spectrometry approaches to facilitate metal-based anticancer drug research, Metallomics 9(4) (2017) 365-381. https://doi.org/10.1039/c6mt00231e
[12] H.U. Holtkamp, C.G. Hartinger, Advanced metallomics methods in anticancer metallodrug mode of action studies, TrAC 104 (2018) 110-117. https://doi.org/10.1016/j.trac.2017.09.023
[13] M. Larroque, S. Mounicou, O. Sgarbura, C. Arnaudguilhem, L. Rebel, C. Leaha, P.-A. Faye, C. Enjalbal, F. Quénet, B. Bouyssiere, S. Carrere, Study of oxaliplatin penetration into ovaries of patients treated with hyperthermic intraperitoneal chemotherapy (HIPEC) for peritoneal metastases of colorectal and appendiceal origin using mass spectrometry imaging, Pleura Peritoneum 6 (2021) 67-74. https://doi.org/10.1515/pp-2020-0149
[14] X. Liu, A.B. Hummon, Chemical Imaging of Platinum-Based Drugs and their Metabolites, Sci. Rep. 6 (2016) 38507. https://doi.org/10.1038/srep38507
[15] A. Bouslimani, N. Bec, M. Glueckmann, C. Hirtz, C. Larroque, Matrix-assisted laser desorption/ionization imaging mass spectrometry of oxaliplatin derivatives in heated intraoperative chemotherapy (HIPEC)-like treated rat kidney, RCM 24(4) (2010) 415-21. https://doi.org/10.1002/rcm.4408
[16] A.B. J. Bianga, N. Bec, F. Quenet, S. Mounicou, B. Bouyssiere, R. Lobinski, J. Szpunar, C. Larroque, Complementary of MALDI and LA ICP mass spectrometry for platinum anticancer imaging in human tumor, Metallomics 6 (2014) 1382-1386. https://doi.org/10.1039/c4mt00131a
[17] M. Aichler, A. Walch, MALDI Imaging mass spectrometry: current frontiers and perspectives in pathology research and practice, Lab. Invest. 95(4) (2015) 422-31. https://doi.org/10.1038/labinvest.2014.156
[18] Y. Fujimura, D. Miura, MALDI Mass Spectrometry Imaging for Visualizing In Situ Metabolism of Endogenous Metabolites and Dietary Phytochemicals, Metabolites 4(2) (2014) 319-46. https://doi.org/10.3390/metabo4020319
[19] D.S. Cornett, S.L. Frappier, R.M. Caprioli, MALDI-FTICR imaging mass spectrometry of drugs and metabolites in tissue, Anal. Chem 80(14) (2008) 5648-53. https://doi.org/10.1021/ac800617s
[20] J. Ferey, F. Marguet, A. Laquerriere, S. Marret, I. Schmitz-Afonso, S. Bekri, C. Afonso, A. Tebani, A new optimization strategy for MALDI FTICR MS tissue analysis for untargeted metabolomics using experimental design and data modeling, Anal. Bioanal. Chem. 411(17) (2019) 3891-3903. https://doi.org/10.1007/s00216-019-01863-6
[21] A. G. Marshall, C. L. Hendrickson, G.S. Jackson, Fourier Transform Ion Cyclotron Resonance Mass Spectrometry: a primer, Mass Spectrom. Rev. 17 (1998) 1-35. https://doi.org/10.1002/(SICI)1098-2787(1998)17:1<1::AID-MAS1>3.0.CO;2-K
[22] F. Xian, C.L. Hendrickson, A.G. Marshall, High resolution mass spectrometry, Anal. Chem. 84(2) (2012) 708-19. https://doi.org/10.1021/ac203191t
[23] Y.H. Kim, Y. Fujimura, T. Hagihara, M. Sasaki, D. Yukihira, T. Nagao, D. Miura, S. Yamaguchi, K. Saito, H. Tanaka, H. Wariishi, K. Yamada, H. Tachibana, In situ label-free imaging for visualizing the

biotransformation of a bioactive polyphenol, Sci. Rep. 3 (2013) 2805.
https://doi.org/10.1038/srep02805
[24] T. Nagao, D. Yukihira, Y. Fujimura, K. Saito, K. Takahashi, D. Miura, H. Wariishi, Power of isotopic fine structure for unambiguous determination of metabolite elemental compositions: in silico evaluation and metabolomic application, Anal. Chim. Acta. 813 (2014) 70-6.
https://doi.org/10.1016/j.aca.2014.01.032
[25] M. Kihara, Y. Matsuo-Tezuka, M. Noguchi-Sasaki, K. Yorozu, M. Kurasawa, Y. Shimonaka, M. Hirata, Visualization of (57)Fe-Labeled Heme Isotopic Fine Structure and Localization of Regions of Erythroblast Maturation in Mouse Spleen by MALDI FTICR-MS Imaging, J. Am. Soc. Mass. Spectrom. 28(11) (2017) 2469-2475. https://doi.org/10.1007/s13361-017-1768-y
[26] L. Xu, X. Li, X. Wang, A. Song, F. Han, A feasible strategy based on isotopic fine structures to enhance the reliability of metabolite identification by Fourier transform ion cyclotron resonance mass spectrometry, Rapid comm in mass spectrom 34(1) (2020) 1-8.
https://doi.org/10.1002/rcm.8560
[27] S.A. Stopka, L.Z. Samarah, J.B. Shaw, A.V. Liyu, D. Velickovic, B.J. Agtuca, C. Kukolj, D.W. Koppenaal, G. Stacey, L. Pasa-Tolic, C.R. Anderton, A. Vertes, Ambient Metabolic Profiling and Imaging of Biological Samples with Ultrahigh Molecular Resolution Using Laser Ablation Electrospray Ionization 21 Tesla FTICR Mass Spectrometry, Anal. Chem. 91(8) (2019) 5028-5035.
https://doi.org/10.1021/acs.analchem.8b05084
[28] D. Elias, B. Raynard, F. Farkhondeh, D. Goéré, D. Rouquie, R. Ciuchendea, M. Pocard, M. Ducreux, Peritoneal carcinomatosis of colorectal origin, Gastroen Clin Biol 30(10) (2006) 1200-1204.
https://doi.org/10.1097/01.sla.0000197702.46394.16
[29] A. Burnett, M. Lecompte, N. Trabulsi, P. Dubé, M. Gervais, B. Trilling, A. Cloutier, L. Sideris, Peritoneal carcinomatosis index predicts survival in colorectal patients undergoing HIPEC using oxaliplatin: a retrospective single-arm cohort study, World J Surg Oncol 17(1) (2019).
https://doi.org/10.1186/s12957-019-1618-4
[30] Y.L. Klaver, T. Hendriks, R.M. Lomme, H.J. Rutten, R.P. Bleichrodt, I.H. de Hingh, Intraoperative versus early postoperative intraperitoneal chemotherapy after cytoreduction for colorectal peritoneal carcinomatosis: an experimental study, Ann. Surg. Oncol. 19 (2012) S475-82.
https://doi.org/10.1245/s10434-011-1984-9
[31] J. Esquivel, D. Elias, D. Baratti, S. Kusamura, M. Deraco, Consensus statement on the loco regional treatment of colorectal cancer with peritoneal dissemination, J. Surg. Oncol. 98(4) (2008) 263-7. https://doi.org/10.1002/jso.21053
[32] T.C. Chua, B.J. Moran, P.H. Sugarbaker, E.A. Levine, O. Glehen, F.N. Gilly, D. Baratti, M. Deraco, D. Elias, A. Sardi, W. Liauw, T.D. Yan, P. Barrios, A. Gomez Portilla, I.H. de Hingh, W.P. Ceelen, J.O. Pelz, P. Piso, S. Gonzalez-Moreno, K. Van Der Speeten, D.L. Morris, Early- and long-term outcome data of patients with pseudomyxoma peritonei from appendiceal origin treated by a strategy of cytoreductive surgery and hyperthermic intraperitoneal chemotherapy, Journal of clinical oncology : official journal of the American Society of Clinical Oncology 30(20) (2012) 2449-56.
https://doi.org/10.1200/JCO.2011.39.7166
[33] F. Quénet, D. Elias, L. Roca, D. Goéré, L. Ghouti, M. Pocard, O. Facy, C. Arvieux, G. Lorimier, D. Pezet, F. Marchal, V. Loi, P. Meeus, B. Juzyna, H. de Forges, J. Paineau, O. Glehen, P. Mariani, C. Brigand, J.-M. Bereder, S. Msika, G. Portier, P. Rat, Cytoreductive surgery plus hyperthermic intraperitoneal chemotherapy versus cytoreductive surgery alone for colorectal peritoneal metastases (PRODIGE 7): a multicentre, randomised, open-label, phase 3 trial, Lancet. Oncol 22(2) (2021) 256-266. https://doi.org/10.1016/S1470-2045(20)30599-4
[34] C. Violette, T. Kim, L. Shandley, R. Lee, C. Staley, J. Winer, S. Maithel, H. Hipp, J. Kawass, M. Russej, Fertility after cytoreductive surgery and hyperthermic intraperitoneal chemotherapy: A call to action, J. Surg. Oncol. 123 (2021) 1045-1049. https://doi.org10.1002/jso.26387
[35] M.W. DeGregorio, D.R. Gandara, W.M. Holleran, E.A. Perez, C.C. King, H.G. Wold, T.J. Montine, R.F. Borch, High-dose cisplatin with diethyldithiocarbamate (DDTC) rescue therapy: preliminary

pharmacologic observations, Cancer Chemother Pharmacol 23 (1989) 276-278. https://doi.org/10.1007/BF00292403
[36] J. Reedijk, Why does cisplatin reach guanine-N7 with competing S-Donor ligands available in the Cell?, Chem. Rev. 99 (1999) 2499-2510. https://doi.org/10.1021/cr980422f
[37] D. Bouvet, A. Michalowicz, S. Crauste-Manciet, D. Brossard, K. Provost, EXAFS and IR structural study of platinum-based anticancer drugs' degradation by diethyl dithiocarbamate, Inorg. Chem. 45 (2006) 3393-3398. https://doi.org/10.1021/ic051904u
[38] D.T. Vengayil, J. Singh, A.L. Singh, V.K. Das, P.B. Singh, Bioaccumulation of carbamate and pyrethroid insecticides in fishes of the river gomti at jaunpur during breeding season, J. Ecophysiol. Occup. Hlth 11 (2011) 1-8. https://doi.org/10.18311/jeoh/2011/2243
[39] S. Soloneski, M. Gonzalez, E. Piaggio, M.A. Reigosa, M.L. Larramendy, Effect of dithiocarbamate pesticide zined and its commercial formulation, azzuro III. Genotoxic evaluation on chinese hamster ovary (CHO) cells, Mutat. Res. (2002) 201-212. https://doi.org/10.1016/s1383-5718(01)00337-0

Figure captions

Figure 1: Structural formulas of oxaliplatin and oxaliplatin-methionine.

Figure 2: MALDI FTICR imaging of ovary tissues before and after HIPEC treatment. Visualization of discriminative values at *m/z* 456.10324, *m/z* 457.10551 and *m/z* 458.10570. Spatial resolution of 120 µm.

Figure 3: MALDI FTICR MS spectra of (a) Experimental and theoretical isotopic distribution patterns of $C_{10}H_{19}N_3O_5Pt$, $C_{11}H_{15}N_7OPt$ and $C_{11}H_{23}N_3S_2Pt$ for M (^{194}Pt), M+1 (^{195}Pt) and M+2 (^{196}Pt) isotopes (b) expanded *m/z* window of the experimental monoisotopic peak at *m/z* 457,10551 and the three theoretical monoisotopic peaks of $C_{10}H_{19}N_3O_5Pt$, $C_{11}H_{15}N_7OPt$ and $C_{11}H_{23}N_3S_2Pt$.

Figure 4: MALDI FTICR MS spectra of observed and theoretical isotopic fine structure of $C_{10}H_{19}N_3O_5Pt$, $C_{11}H_{15}N_7OPt$ and $C_{11}H_{23}N_3S_2Pt$ for M+2 (^{196}Pt).

Table captions

Table 1: Theoretical *m/z* values of the isotopes M (^{194}Pt), M+1 (^{195}Pt) and M+2 (^{196}Pt) for oxaliplatin and oxaliplatin-methionine complex.

Table 2: Theoretical and experimental *m/z* values and relative abundance (%) of the isotopes M (^{194}Pt), M+1 (^{195}Pt) and M+2 (^{196}Pt) for the determined raw formulas $C_{10}H_{19}N_3O_5Pt$, $C_{11}H_{15}N_7OPt$ and $C_{11}H_{23}N_3S_2Pt$ and the unknown compound with associated *m/z* errors.